

# Séminaire Laurent Schwartz

## EDP et applications

Année 2017-2018


Kazuo Aoki and Shingo Kosuge

**Shock wave structure for polyatomic gases with large bulk viscosities**

*Séminaire Laurent Schwartz — EDP et applications* (2017-2018), Exposé n° VII, 18 p.

[http://sisedp.cedram.org/item?id=SLSEDP\\_2017-2018\\_\\_\\_\\_A7\\_0](http://sisedp.cedram.org/item?id=SLSEDP_2017-2018____A7_0)

© Institut des hautes études scientifiques & Centre de mathématiques Laurent Schwartz,  
École polytechnique, 2017-2018.

 Cet article est mis à disposition selon les termes de la licence  
CREATIVE COMMONS ATTRIBUTION – PAS DE MODIFICATION 3.0 FRANCE.  
<http://creativecommons.org/licenses/by-nd/3.0/fr/>

Institut des hautes études scientifiques  
Le Bois-Marie • Route de Chartres  
F-91440 BURES-SUR-YVETTE  
<http://www.ihes.fr/>

Centre de mathématiques Laurent Schwartz  
CMLS, École polytechnique, CNRS, Université  
Paris-Saclay  
F-91128 PALAISEAU CEDEX  
<http://www.math.polytechnique.fr/>

**cedram**

*Exposé mis en ligne dans le cadre du*  
*Centre de diffusion des revues académiques de mathématiques*  
<http://www.cedram.org/>

# Shock Wave Structure for Polyatomic Gases with Large Bulk Viscosities

Kazuo Aoki<sup>1</sup> and Shingo Kosuge<sup>2</sup>

<sup>1</sup>Department of Mathematics, National Cheng Kung University,  
Tainan 70101, Taiwan and National Center for Theoretical Sciences,  
National Taiwan University, Taipei 10617, Taiwan

<sup>2</sup>Institute for Liberal Arts and Sciences, Kyoto University,  
Kyoto 606-8501, Japan

**Abstract** The structure of a standing plane shock wave in a polyatomic gas is investigated on the basis of kinetic theory, with special interest in gases with large bulk viscosities, such as CO<sub>2</sub> gas. The ellipsoidal statistical (ES) model for a polyatomic gas is employed. First, the shock structure is computed numerically for different upstream Mach numbers and for different (large) values of the ratio of the bulk viscosity to the shear viscosity, and the double-layer structure consisting of a thin upstream layer with a steep change and a much thicker downstream layer with a mild change is obtained. Then, an asymptotic analysis for large values of the ratio is carried out, and an analytical solution that describes the thick downstream layer correctly is obtained.

## 1 Introduction

A shock wave is described as a discontinuous surface, across which the density, the velocity normal to the surface, and the temperature of a gas exhibit jumps, in inviscid gas dynamics. In reality, however, the shock wave has a structure, that is, physical quantities undergo steep but continuous changes across a thin layer of thickness of a few mean free paths. To describe such a structure, one has to use, in principle, kinetic theory of gases instead of ordinary gas dynamics. The structure of a standing plane shock wave is one of the most fundamental problems in kinetic theory and has been investigated by many authors (see, e.g., [1, 2, 3, 4, 5]). In the present study, we consider this classical problem with special interest in polyatomic gases with large bulk viscosities, such as carbon dioxide (CO<sub>2</sub>) gas.

Recently, the shock-structure problem was investigated for polyatomic gases on the basis of extended thermodynamics [6, 7], and some interesting results were obtained. In [6], it was shown that for CO<sub>2</sub> gas, macroscopic quantities exhibit profiles of three different types (Types A, B, and C in [6, 7]) depending on the upstream Mach number. When the Mach number is very close to 1, i.e., the shock wave is very weak, the profiles of the density, velocity, and temperature are almost symmetric with respect to the centers of the respective profiles (Type A). When the Mach number is increased slightly, the profiles become nonsymmetric and exhibit

a corner upstream (Type B). If the Mach number is increased slightly more, one obtains profiles with a double-layer structure, consisting of a thin front layer with a steep change and a thick rear layer over which the quantities slowly approach the downstream equilibrium values (Type C).

However, these results are based on extended thermodynamics, which is essentially a macroscopic theory. Since the problem is basically for kinetic theory as mentioned at the beginning, they also need to be justified directly from kinetic theory. This is the motivation of the present study. However, kinetic approach is not an easy task because of the extreme complexity of the collision integral of the Boltzmann equation for a polyatomic gas. Therefore, we adopt the polyatomic version of the ellipsoidal statistical (ES) model, which was proposed in [8] and was rederived in a systematic way in [9].

In the present study, we first show that the three types of shock profiles (Type A, Type B, and Type C) are also obtained by the direct numerical analysis of the ES model. Then, we carry out an asymptotic analysis for large bulk viscosity based on the ES model to obtain an analytical solution that describes the thick rear layer of Type C correctly. This analytical solution also describes the entire profiles of Type A and Type B. Since the details of the numerical and asymptotic analyses are found in [10], we only summarize necessary materials and main results in the present note.

## 2 Problem

Let us consider a stationary plane shock wave standing in a flow of an ideal polyatomic gas. We take the  $X_1$  axis of the coordinate system  $(X_1, X_2, X_3)$  perpendicular to the shock wave. The gas at upstream infinity ( $X_1 \rightarrow -\infty$ ) is in an equilibrium state with density  $\rho_-$ , flow velocity  $\mathbf{v}_- = (v_-, 0, 0)$ , and temperature  $T_-$ , and that at downstream infinity ( $X_1 \rightarrow \infty$ ) is in another equilibrium state with density  $\rho_+$ , flow velocity  $\mathbf{v}_+ = (v_+, 0, 0)$ , and temperature  $T_+$ . We investigate the steady behavior of the gas assuming that the problem is spatially one dimensional and using the ES model for a polyatomic gas [8, 9].

Let us denote by  $\gamma$  the ratio of the specific heats ( $\gamma = c_p/c_v$ , where  $c_p$  and  $c_v$  are the specific heat at constant pressure and that at constant volume, respectively) and assume that  $c_p$ ,  $c_v$ , and thus  $\gamma$  are constant (*calorically perfect gas*). Then,  $\gamma$  is expressed in terms of the internal degrees of freedom  $\delta$  of a molecule as

$$\gamma = (\delta + 5)/(\delta + 3). \quad (1)$$

We denote by  $M_-$  the Mach number of the flow at upstream infinity, i.e.,  $M_- = v_-/\sqrt{\gamma RT_-}$ , where  $R$  is the gas constant per unit mass ( $R = k/m$  with the Boltzmann constant  $k$  and the mass of a molecule  $m$ ). Then, the Rankine–Hugoniot relations give the following expressions of the downstream quantities  $\rho_+$ ,  $v_+$ , and  $T_+$  in terms of the upstream quantities  $\rho_-$ ,  $v_-$ , and  $T_-$  and the upstream Mach

number  $M_-$ :

$$\rho_+ = \frac{(\gamma + 1)M_-^2}{(\gamma - 1)M_-^2 + 2} \rho_-, \quad (2a)$$

$$v_+ = \frac{(\gamma - 1)M_-^2 + 2}{(\gamma + 1)M_-^2} v_-, \quad (2b)$$

$$T_+ = \frac{[2\gamma M_-^2 - (\gamma - 1)][(\gamma - 1)M_-^2 + 2]}{(\gamma + 1)^2 M_-^2} T_-. \quad (2c)$$

### 3 Basic equations

Let  $t$  be the time variable,  $\mathbf{X}$  (or  $X_i$ ) the position vector in the physical space,  $\boldsymbol{\xi}$  (or  $\xi_i$ ) the molecular velocity, and  $\mathcal{E}$  the energy per unit mass associated with the internal modes. We denote the number of the gas molecules contained in an infinitesimal volume  $d\mathbf{X}d\boldsymbol{\xi}d\mathcal{E}$  around a point  $(\mathbf{X}, \boldsymbol{\xi}, \mathcal{E})$  in the seven-dimensional space  $(\mathbf{X}, \boldsymbol{\xi}, \mathcal{E})$  at time  $t$  by  $(1/m)f(t, \mathbf{X}, \boldsymbol{\xi}, \mathcal{E})d\mathbf{X}d\boldsymbol{\xi}d\mathcal{E}$ . The function  $f(t, \mathbf{X}, \boldsymbol{\xi}, \mathcal{E})$ , which may be called the velocity/energy distribution function of gas molecules, is the fundamental physical quantity and is governed by the ES model. In the present time-independent and spatially one-dimensional case, where  $f = f(X_1, \boldsymbol{\xi}, \mathcal{E})$ , the equation is written in the following form:

$$\xi_1 \frac{\partial f}{\partial X_1} = Q(f), \quad (3)$$

where

$$Q(f) = A_c(T)\rho(\mathcal{G} - f), \quad (4a)$$

$$\mathcal{G} = \frac{\rho \mathcal{E}^{\delta/2-1}}{(2\pi)^{3/2} [\det(\mathbb{T})]^{1/2} (RT_{\text{rel}})^{\delta/2} \Gamma(\delta/2)} \times \exp\left(-\frac{1}{2}(\xi_i - v_i)(\mathbb{T}^{-1})_{ij}(\xi_j - v_j) - \frac{\mathcal{E}}{RT_{\text{rel}}}\right), \quad (4b)$$

$$(\mathbb{T})_{ij} = (1 - \theta)[(1 - \nu)RT_{\text{tr}}\delta_{ij} + \nu p_{ij}/\rho] + \theta RT\delta_{ij}, \quad (4c)$$

$$\rho = \iint_0^\infty f d\mathcal{E} d\boldsymbol{\xi}, \quad (4d)$$

$$v_i = \frac{1}{\rho} \iiint_0^\infty \xi_i f d\mathcal{E} d\boldsymbol{\xi}, \quad (4e)$$

$$p_{ij} = \iint_0^\infty (\xi_i - v_i)(\xi_j - v_j) f d\mathcal{E} d\boldsymbol{\xi}, \quad (4f)$$

$$T_{\text{tr}} = \frac{1}{3\rho R} \iint_0^\infty |\boldsymbol{\xi} - \mathbf{v}|^2 f d\mathcal{E} d\boldsymbol{\xi}, \quad (4g)$$

$$T_{\text{int}} = \frac{2}{\delta\rho R} \iint_0^\infty \mathcal{E} f d\mathcal{E} d\boldsymbol{\xi}, \quad (4h)$$

$$T = \frac{3T_{\text{tr}} + \delta T_{\text{int}}}{3 + \delta}, \quad (4i)$$

$$T_{\text{rel}} = \theta T + (1 - \theta)T_{\text{int}}. \quad (4j)$$

Here,  $\rho$  is the density,  $\mathbf{v}$  (or  $v_i$ ) =  $(v_1, 0, 0)$  the flow velocity,  $p_{ij}$  the stress tensor,  $T_{\text{tr}}$  the temperature associated with translational motion,  $T_{\text{int}}$  the temperature associated with the energy of the internal modes,  $T$  the temperature,  $d\boldsymbol{\xi} = d\xi_1 d\xi_2 d\xi_3$ , and the domain of integration with respect to  $\boldsymbol{\xi}$  is the whole space of  $\boldsymbol{\xi}$ . The symbol  $\delta_{ij}$  indicates the Kronecker delta, and  $\nu \in [-1/2, 1)$  and  $\theta \in (0, 1]$  are the constants that adjust the Prandtl number and the bulk viscosity. In addition,  $A_c(T)$  is a function of  $T$  such that  $A_c(T)\rho$  is the collision frequency of the gas molecules,  $\Gamma(z)$  is the gamma function defined by

$$\Gamma(z) = \int_0^\infty s^{z-1} e^{-s} ds, \quad (5)$$

$\mathbb{T}$  is the  $3 \times 3$  positive-definite symmetric matrix whose  $(i, j)$  component is defined by Eq. (4c), and  $\det(\mathbb{T})$  and  $\mathbb{T}^{-1}$  are, respectively, its determinant and inverse. In Eq. (4b), the summation convention  $a_i c_{ij} b_j = \sum_{i,j=1}^3 a_i c_{ij} b_j$  is used.

The boundary condition at upstream infinity and that at downstream infinity are given as follows:

$$f = \frac{\rho_- \mathcal{E}^{\delta/2-1}}{(2\pi RT_-)^{3/2} (RT_-)^{\delta/2} \Gamma(\delta/2)} \times \exp\left(-\frac{(\xi_1 - v_-)^2 + \xi_2^2 + \xi_3^2}{2RT_-} - \frac{\mathcal{E}}{RT_-}\right), \quad (X_1 \rightarrow -\infty), \quad (6a)$$

$$f = \frac{\rho_+ \mathcal{E}^{\delta/2-1}}{(2\pi RT_+)^{3/2} (RT_+)^{\delta/2} \Gamma(\delta/2)} \times \exp\left(-\frac{(\xi_1 - v_+)^2 + \xi_2^2 + \xi_3^2}{2RT_+} - \frac{\mathcal{E}}{RT_+}\right), \quad (X_1 \rightarrow \infty). \quad (6b)$$

It should be mentioned that for Eq. (3), the viscosity  $\mu$ , the thermal conductivity  $\kappa$ , the Prandtl number  $\text{Pr}$ , and the bulk viscosity  $\mu_b$  are obtained as

$$\mu = \frac{1}{1 - \nu + \theta\nu} \frac{RT}{A_c(T)}, \quad \kappa = \frac{\gamma R}{\gamma - 1} \frac{RT}{A_c(T)}, \quad (7a)$$

$$\text{Pr} = \frac{1}{1 - \nu + \theta\nu}, \quad \mu_b = \frac{1}{\theta} \left(\frac{5}{3} - \gamma\right) \frac{\mu}{\text{Pr}}. \quad (7b)$$

## 4 Numerical analysis

One of the advantages of using the ES model is that one can reduce the independent variables from  $(X_1, \xi_1, \xi_2, \xi_3, \mathcal{E})$  to  $(X_1, \xi_1)$  eliminating the molecular velocity components  $\xi_2$  and  $\xi_3$  parallel to the shock and the energy variable  $\mathcal{E}$  in the present

spatially one-dimensional problem. More specifically, we introduce the following three marginal velocity distribution functions:

$$g(X_1, \xi_1) = \iint_{-\infty}^{\infty} \int_0^{\infty} f(X_1, \xi_1, \xi_2, \xi_3, \mathcal{E}) d\mathcal{E} d\xi_2 d\xi_3, \quad (8a)$$

$$h(X_1, \xi_1) = \iint_{-\infty}^{\infty} \int_0^{\infty} (\xi_2^2 + \xi_3^2) f(X_1, \xi_1, \xi_2, \xi_3, \mathcal{E}) d\mathcal{E} d\xi_2 d\xi_3, \quad (8b)$$

$$i(X_1, \xi_1) = \iint_{-\infty}^{\infty} \int_0^{\infty} \mathcal{E} f(X_1, \xi_1, \xi_2, \xi_3, \mathcal{E}) d\mathcal{E} d\xi_2 d\xi_3. \quad (8c)$$

If we multiply Eq. (3) by 1,  $\xi_2^2 + \xi_3^2$ , and  $\mathcal{E}$  and integrate the respective results over  $-\infty < \xi_2, \xi_3 < \infty$  and  $0 < \mathcal{E} < \infty$ , then we obtain three simultaneous integro-differential equations of ES type for  $g$ ,  $h$ , and  $i$ . It should be noted that the resulting equations do not contain the energy variable  $\mathcal{E}$  associated with the internal degrees of freedom. The boundary conditions for these equations at  $X_1 \rightarrow \pm\infty$  can be obtained by a similar procedure. Here, we omit the resulting equations and boundary conditions (see [10]).

The equations for  $g$ ,  $h$ , and  $i$  are solved numerically by an iterative finite-different method. The details of the method, as well as the data for the computational systems (the distribution of the grid points, the ranges for the variables in the computation, etc.), are shown in [10], so that we omit them here and only show the results.

## 5 Numerical results

Let us restrict ourselves to CO<sub>2</sub> gas. We set  $\delta = 4$  and  $\text{Pr} = 0.761$  and assume that  $A_c(T) = \text{const}$ , referring basically to [11]. We also let  $T_- = 293\text{K}$ . According to [12], the ratio  $\mu_b/\mu$  is large and between  $10^3$  and  $4 \times 10^3$  at this temperature. In the present study, in order to observe the change of the shock profiles as  $\mu_b/\mu$  increases, we carried out computation for  $\mu_b/\mu$  varying from 100 to 2000. In this sense, our CO<sub>2</sub> gas is a *pseudo*-CO<sub>2</sub> gas with variable  $\mu_b/\mu$ .

In the following, the results are shown for  $M_- = 5$ , 1.138..., and 1.05. We show the profiles of the density  $\rho$ , the flow velocity  $v_1$  (the  $X_1$  component), and the temperatures  $T$  normalized in the conventional way, that is,

$$\check{\rho} = \frac{\rho - \rho_-}{\rho_+ - \rho_-}, \quad \check{v} = \frac{v_1 - v_+}{v_- - v_+}, \quad \check{T} = \frac{T - T_-}{T_+ - T_-}. \quad (9)$$

In the figures shown in the following (except for Fig. 2), the coordinate  $x_1$  is the dimensionless coordinate normalized by the mean free path  $l_-$  at the equilibrium state at rest with density  $\rho_-$  and temperature  $T_-$ , that is,

$$x_1 = X_1/l_-, \quad l_- = (2/\sqrt{\pi})(2RT_-)^{1/2}/A_c(T_-)\rho_-. \quad (10)$$

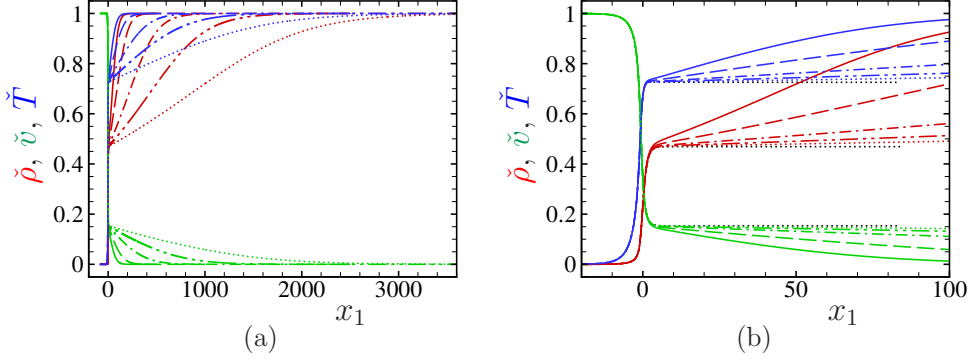


Fig. 1: Profiles of  $\check{\rho}$ ,  $\check{v}$ , and  $\check{T}$  at  $M_- = 5$  for  $\delta = 4$ ,  $\text{Pr} = 0.761$ ,  $A_c = \text{const}$ , and  $\mu_b/\mu = 100, 200, 500, 1000$ , and  $2000$ . (a) Profiles for  $-200 \leq x_1 \leq 3600$ , (b) profiles for  $-20 \leq x_1 \leq 100$ . The red curves indicate  $\check{\rho}$ , the green curves  $\check{v}$ , and the blue curves  $\check{T}$ . The solid lines indicate the profiles for  $\mu_b/\mu = 100$ , the dashed lines for  $\mu_b/\mu = 200$ , the dot-dashed lines for  $\mu_b/\mu = 500$ , the dot-dot-dashed lines for  $\mu_b/\mu = 1000$ , and the dotted lines for  $\mu_b/\mu = 2000$ . In panel (b), the black dotted lines indicate the profiles of  $\check{\rho}$ ,  $\check{v}$ , and  $\check{T}$  for  $\mu_b/\mu = \infty$ .

• Case of  $M_- = 5$

Figure 1 shows the profiles of  $\check{\rho}$ ,  $\check{v}$ , and  $\check{T}$  at  $M_- = 5$  for  $\text{CO}_2$  gas with  $\mu_b/\mu = 100, 200, 500, 1000$ , and  $2000$ . Figure 1(b) is a magnified figure of Fig. 1(a) in the range  $-20 \leq x_1 (= X_1/l_-) \leq 100$ . The red curves indicate  $\check{\rho}$ , the green curves  $\check{v}$ , and the blue curves  $\check{T}$ ; the solid lines indicate  $\mu_b/\mu = 100$ , the dashed lines  $\mu_b/\mu = 200$ , the dot-dashed lines  $\mu_b/\mu = 500$ , the dot-dot-dashed lines  $\mu_b/\mu = 1000$ , and the dotted lines  $\mu_b/\mu = 2000$ . In Fig. 1(b), we also show by the black dotted lines the profiles of  $\check{\rho}$ ,  $\check{v}$ , and  $\check{T}$  when  $\mu_b/\mu = \infty$ . In this case, since  $\theta = 0$  [cf. Eq. (7b)], there is no relaxation between  $T_{\text{tr}}$  and  $T_{\text{int}}$  through  $T$  [cf. Eqs. (4c) and (4j)]. Therefore, the downstream condition is different from Eq. (6b) and is given by

$$f = \frac{\tilde{\rho}_+ \mathcal{E}^{\delta/2-1}}{(2\pi R \tilde{T}_{\text{tr}+})^{3/2} (R \tilde{T}_{\text{int}+})^{\delta/2} \Gamma(\delta/2)} \times \exp\left(-\frac{(\xi_1 - \tilde{v}_+)^2 + \xi_2^2 + \xi_3^2}{2R \tilde{T}_{\text{tr}+}} - \frac{\mathcal{E}}{R \tilde{T}_{\text{int}+}}\right), \quad (X_1 \rightarrow \infty), \quad (11)$$

where  $\tilde{\rho}_+$ ,  $\tilde{v}_+$ ,  $\tilde{T}_{\text{tr}+}$ , and  $\tilde{T}_{\text{int}+}$  are given by

$$\tilde{\rho}_+ = \frac{4\tilde{M}_-^2}{\tilde{M}_-^2 + 3} \rho_-, \quad \tilde{v}_+ = \frac{\tilde{M}_-^2 + 3}{4\tilde{M}_-^2} v_-, \quad (12a)$$

$$\tilde{T}_{\text{tr}+} = \frac{(5\tilde{M}_-^2 - 1)(\tilde{M}_-^2 + 3)}{16\tilde{M}_-^2} T_-, \quad \tilde{T}_{\text{int}+} = T_-, \quad (12b)$$

$$\tilde{M}_- = v_- / \sqrt{5RT_-/3} = M_- \sqrt{3\gamma/5}, \quad (12c)$$

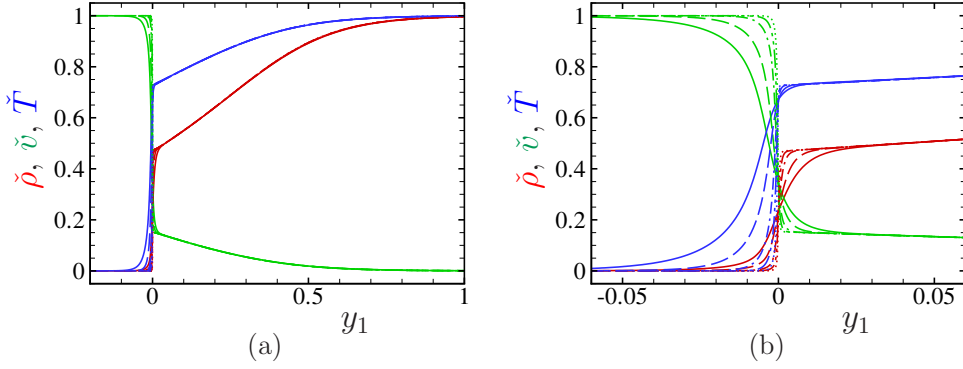


Fig. 2: Profiles of  $\check{\rho}$ ,  $\check{v}$ , and  $\check{T}$  at  $M_- = 5$  for  $\delta = 4$ ,  $\text{Pr} = 0.761$ ,  $A_c = \text{const}$ , and  $\mu_b/\mu = 100, 200, 500, 1000$ , and  $2000$  in the new coordinate  $y_1$ . (a) Profiles for  $-0.2 \leq y_1 \leq 1$ , (b) profiles for  $-0.06 \leq y_1 \leq 0.06$ . The red curves indicate  $\check{\rho}$ , the green curves  $\check{v}$ , and the blue curves  $\check{T}$ . See the caption of Fig. 1 about the types of lines.

and the temperature at downstream infinity is given by  $T = (3\tilde{T}_{\text{tr}+} + \delta\tilde{T}_{\text{int}+})/(3 + \delta)$  Equation (12) is the Rankine–Hugoniot relations for  $\mu_b/\mu = \infty$ . Note that it is the same as the Rankine–Hugoniot relations for a monatomic gas if  $\tilde{M}_-$  is regarded as the upstream Mach number. In Fig. 1,  $x_1 = 0$  is set at the position where the density is equal to the average of the upstream and downstream values when  $\mu_b/\mu = \infty$ , that is,  $\rho = (\rho_- + \tilde{\rho}_+)/2$ .

The profiles in Fig. 1 are of Type C consisting of a thin front layer and a thick rear layer. As  $\mu_b/\mu$  increases, the thickness of the rear layer increases and reaches over 3000 mean free paths ( $l_-$ ), whereas the profiles of the thin front layer are not affected by  $\mu_b/\mu$  and coincide with the shock profiles for  $\mu_b/\mu = \infty$ . This indicates that the thin front layer corresponds to the shock wave for  $\mu_b/\mu = \infty$ , and the jump caused by this layer is given by the Rankine–Hugoniot relations for  $\mu_b/\mu = \infty$ . Therefore, Type-C profile should appear when  $\tilde{M}_- > 1$ .

Here, we introduce the new space coordinate  $y_1$  whose length scale of variation is  $l_-/\theta$ , i.e.,

$$y_1 = (2/\sqrt{\pi})\theta x_1 = (2/\sqrt{\pi})\theta(X_1/l_-), \quad (13)$$

which is expected to describe the slow variation occurring in the thick rear layer when  $\mu_b/\mu \gg 1$  ( $\theta \ll 1$ ). In Fig. 2, we show the profiles of  $\check{\rho}$ ,  $\check{v}$ , and  $\check{T}$ , corresponding to Fig. 1, as the functions of  $y_1$ . Figure 2(b) is a magnified figure of Fig. 2(a). As one can see, the curves for  $\mu_b/\mu = 100, 200, 500, 1000$ , and  $2000$  coincide perfectly in the thick rear layer. Using this new coordinate  $y_1$ , we will derive a set of macroscopic equations that can describe the slow relaxation over the thick rear layer in Sec. 6.1.

- Case of  $M_- = 1.138\dots$

This case corresponds to  $\tilde{M}_- = 1$ , at which the thin front layer of Type-C profile disappears. Figure 3 shows the profiles of  $\check{\rho}$ ,  $\check{v}$ , and  $\check{T}$ , and Fig. 3(b) is the magnified



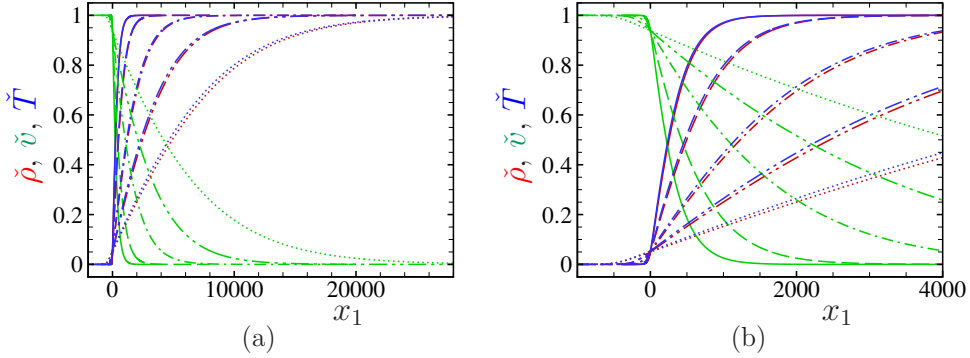


Fig. 3: Profiles of  $\check{\rho}$ ,  $\check{v}$ , and  $\check{T}$  at  $M_- = 1.138\dots$  ( $\widetilde{M}_- = 1$ ) for  $\delta = 4$ ,  $\text{Pr} = 0.761$ ,  $A_c = \text{const}$ , and  $\mu_b/\mu = 100, 200, 500, 1000$ , and  $2000$ . (a) Profiles for  $-2000 \leq x_1 \leq 28000$ , (b) profiles for  $-1000 \leq x_1 \leq 4000$ . The red curves indicate  $\check{\rho}$ , the green curves  $\check{v}$ , and the blue curves  $\check{T}$ . The solid lines indicate the profiles for  $\mu_b/\mu = 100$ , the dashed lines for  $\mu_b/\mu = 200$ , the dot-dashed lines for  $\mu_b/\mu = 500$ , the dot-dot-dashed lines for  $\mu_b/\mu = 1000$ , and the dotted lines for  $\mu_b/\mu = 2000$ .

figure of Figs. 3(a). In the figure,  $x_1 = 0$  is set at the position where  $\check{\rho} = 0.05$ . The profiles do not show the double layer structure, but the thickness of the shock increases as  $\mu_b/\mu$  becomes large, as in the case of  $M_- = 5$ . The profiles start abruptly from the upstream uniform state though the approach of the profiles to the downstream uniform state is slow and smooth. Therefore, the profiles are not symmetric with respect to the centers of the respective profiles, and we can say that the profiles in this case are of Type B.

- Case of  $M_- = 1.05$

Finally, we show the profiles of  $\check{\rho}$ ,  $\check{v}$ , and  $\check{T}$  for  $M_- = 1.05$  in Fig. 4. Figure 4(b) is a magnified figure of Fig. 4(a). In the figure,  $x_1 = 0$  is set at the position where  $\check{\rho} = 1/2$ . The profiles, which are almost symmetric with respect to the centers of respective profiles, correspond to Type-A profile. The thickness of the shock increases with the increase of  $\mu_b/\mu$  and reaches over 50000 mean free paths for  $\mu_b/\mu = 2000$ .

In this way, the transition of the profiles from Type A to Type C, which was predicted by the extended thermodynamics [6], is also observed in the present computation based on the ES model.

## 6 Asymptotic analysis for large $\mu_b/\mu$

### 6.1 Slowly-varying solution

Figure 2 in Sec. 5 suggests that the thick layer behind the thin layer of Type-C profile for large  $\mu_b/\mu$  (i.e., small  $\theta$ ) may be described by a slowly-varying solution

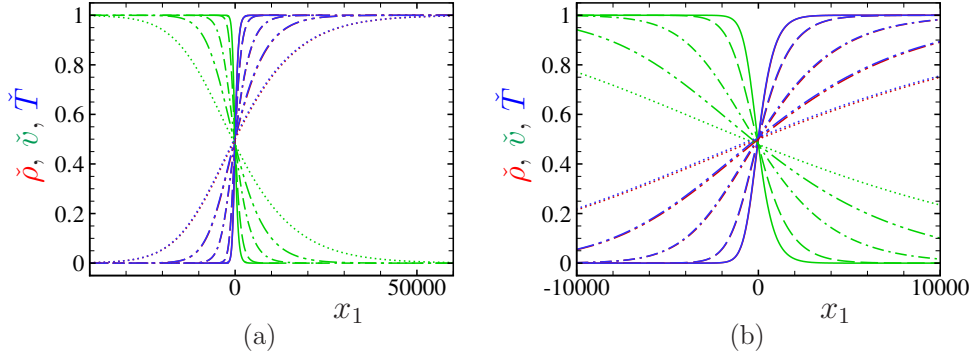


Fig. 4: Profiles of  $\hat{\rho}$ ,  $\hat{v}$ , and  $\hat{T}$  at  $M_- = 1.05$  for  $\delta = 4$ ,  $\text{Pr} = 0.761$ ,  $A_c = \text{const}$ , and  $\mu_b/\mu = 100, 200, 500, 1000$ , and  $2000$ . (a) Profiles for  $-40000 \leq x_1 \leq 60000$ , (b) profiles for  $-10000 \leq x_1 \leq 10000$ . The red curves indicate  $\hat{\rho}$ , the green curves  $\hat{v}$ , and the blue curves  $\hat{T}$ . The solid lines indicate the profiles for  $\mu_b/\mu = 100$ , the dashed lines for  $\mu_b/\mu = 200$ , the dot-dashed lines for  $\mu_b/\mu = 500$ , the dot-dot-dashed lines for  $\mu_b/\mu = 1000$ , and the dotted lines for  $\mu_b/\mu = 2000$ .

whose length scale of variation is of the order  $l_-/\theta$ . Although the results are not shown in Sec. 5, the replot of the curves in Figs. 3 and 4 in terms of the variable  $y_1$  [Eq. (13)] shows that the profiles of each macroscopic quantity for large  $\mu_b/\mu$  fall on a single curve for respective  $M_-$ . Therefore, we expect that the slowly-varying solution may also describe the whole profiles of Types A and B.

Let us introduce the dimensionless quantities  $[\zeta_i, \hat{\mathcal{E}}, \hat{f}, \hat{\mathcal{G}}, \hat{A}_c(\hat{T}), \hat{\rho}, \hat{v}_i, \hat{p}_{ij}, \hat{T}_{\text{tr}}, \hat{T}_{\text{int}}, \hat{T}, \hat{T}_{\text{rel}}]$ , which correspond to the original dimensional quantities  $[\xi_i, \mathcal{E}, f, \mathcal{G}, A_c(T), \rho, v_i, p_{ij}, T_{\text{tr}}, T_{\text{int}}, T, T_{\text{rel}}]$ , by the following relations:

$$\begin{aligned} \zeta_i &= \xi_i/(2RT_-)^{1/2}, & \hat{\mathcal{E}} &= \mathcal{E}/RT_-, \\ (\hat{f}, \hat{\mathcal{G}}) &= (f, \mathcal{G})/2\rho_-(2RT_-)^{-5/2}, & \hat{A}_c(\hat{T}) &= A_c(T)/A_c(T_-), \\ \hat{\rho} &= \rho/\rho_-, & \hat{v}_i &= v_i/(2RT_-)^{1/2}, & \hat{p}_{ij} &= p_{ij}/p_-, \\ (\hat{T}_{\text{tr}}, \hat{T}_{\text{int}}, \hat{T}, \hat{T}_{\text{rel}}) &= (T_{\text{tr}}, T_{\text{int}}, T, T_{\text{rel}})/T_-, \end{aligned} \quad (14)$$

where  $p_- = R\rho_-T_-$ . If we assume that  $\hat{f}$  is slowly varying, i.e., a function of the variable  $y_1$  [Eq. (13)]:  $\hat{f} = \hat{f}(y_1, \zeta, \hat{\mathcal{E}})$ , then we have the dimensionless ES model of the following form:

$$\theta\zeta_1 \frac{\partial \hat{f}}{\partial y_1} = \hat{A}_c(\hat{T})\hat{\rho}(\hat{\mathcal{G}} - \hat{f}). \quad (15)$$

The explicit form of  $\hat{\mathcal{G}}$ , which is almost the same as  $\mathcal{G}$  in Eq. (4b), is omitted here (see [10]).

We analyze Eq. (15) for  $\theta \ll 1$  by a Hilbert-type expansion in  $\theta$ , i.e.,

$$\hat{f} = \hat{f}^{(0)} + \hat{f}^{(1)}\theta + \hat{f}^{(2)}\theta^2 + \dots \quad (16)$$

Correspondingly, the macroscopic quantities  $h$  ( $h = \hat{\rho}, \hat{v}_1, \hat{p}_{ij}, \dots$ ) are also expanded as

$$\hat{h} = \hat{h}^{(0)} + \hat{h}^{(1)}\theta + \hat{h}^{(2)}\theta^2 + \dots \quad (17)$$

We leave the details of the analysis in Appendix C of [10], where the three-dimensional version of Eq. (15) is analyzed. As the result of the analysis, the macroscopic equations that describe the leading-order quantities  $\hat{\rho}^{(0)}$ ,  $\hat{v}_1^{(0)}$ ,  $\hat{T}_{\text{tr}}^{(0)}$ , and  $\hat{T}_{\text{int}}^{(0)}$  of the expansion (17) are obtained. We omit the superscript (0) for brevity. Then, we have the following system of ordinary differential equations for  $\hat{\rho}$ ,  $\hat{v}_1$ ,  $\hat{T}_{\text{tr}}$ , and  $\hat{T}_{\text{int}}$ :

$$\frac{d}{dy_1} (\hat{\rho}\hat{v}_1) = 0, \quad (18a)$$

$$\frac{d}{dy_1} \left( \frac{\hat{T}_{\text{tr}}}{\hat{v}_1} + 2\hat{v}_1 \right) = 0, \quad (18b)$$

$$\frac{d}{dy_1} \left( \hat{v}_1^2 + \frac{5}{2}\hat{T}_{\text{tr}} + \frac{\delta}{2}\hat{T}_{\text{int}} \right) = 0, \quad (18c)$$

$$\hat{v}_1 \frac{d\hat{T}_{\text{int}}}{dy_1} = \frac{3}{3+\delta} \hat{A}_c(\hat{T}) \hat{\rho} (\hat{T}_{\text{tr}} - \hat{T}_{\text{int}}), \quad (18d)$$

where  $\hat{T}$  in  $\hat{A}_c(\hat{T})$  is given by

$$\hat{T} = \frac{3\hat{T}_{\text{tr}} + \delta\hat{T}_{\text{int}}}{3+\delta}, \quad (19)$$

which is the dimensionless version of Eq. (4i).

It should be noted that  $(\hat{\rho}, \hat{v}_1, \hat{T}_{\text{tr}}, \hat{T}_{\text{int}})$  are equal to  $(1, \hat{v}_-, 1, 1)$  at upstream infinity and to  $(\hat{\rho}_+, \hat{v}_+, \hat{T}_+, \hat{T}_+)$  at downstream infinity, where

$$\hat{v}_{\pm} = \frac{v_{\pm}}{(2RT_-)^{1/2}}, \quad \hat{\rho}_+ = \frac{\rho_+}{\rho_-}, \quad \hat{T}_+ = \frac{T_+}{T_-}. \quad (20)$$

and they are related by the dimensionless version of the Rankine–Hugoniot relations (2) or the original conservation laws

$$\hat{\rho}_+ \hat{v}_+ = \hat{v}_-, \quad \frac{\hat{T}_+}{\hat{v}_+} + 2\hat{v}_+ = \frac{1}{\hat{v}_-} + 2\hat{v}_-, \quad \hat{v}_+^2 + \frac{5+\delta}{2}\hat{T}_+ = \hat{v}_-^2 + \frac{5+\delta}{2}. \quad (21)$$

It follows from Eqs. (18a)–(18c) that

$$\hat{\rho}\hat{v}_1 = c_1, \quad \frac{\hat{T}_{\text{tr}}}{\hat{v}_1} + 2\hat{v}_1 = c_2, \quad \hat{v}_1^2 + \frac{5}{2}\hat{T}_{\text{tr}} + \frac{\delta}{2}\hat{T}_{\text{int}} = c_3, \quad (22)$$

where  $c_1$ ,  $c_2$ , and  $c_3$  are constants, or

$$\hat{\rho} = \frac{c_1}{\hat{v}_1}, \quad \hat{T}_{\text{tr}} = \hat{v}_1 (c_2 - 2\hat{v}_1), \quad \hat{T}_{\text{int}} = \frac{2}{\delta} \left( c_3 - \frac{5}{2}c_2\hat{v}_1 + 4\hat{v}_1^2 \right). \quad (23)$$

The substitution of Eq. (23) into Eq. (18d) with Eq. (19) gives the following equation for  $\widehat{v}_1$ :

$$\widehat{v}_1^2 \left( \frac{5}{16} c_2 - \widehat{v}_1 \right) \frac{d\widehat{v}_1}{dy_1} = \frac{3(4+\delta)}{8(3+\delta)} c_1 \widehat{A}_c(\widehat{T}) \left[ \widehat{v}_1^2 - \frac{5+\delta}{2(4+\delta)} c_2 \widehat{v}_1 + \frac{c_3}{4+\delta} \right], \quad (24a)$$

$$\widehat{T} = \frac{2}{3+\delta} (\widehat{v}_1^2 - c_2 \widehat{v}_1 + c_3). \quad (24b)$$

In the case of the Type-C profile, the slowly-varying solution should be applied to the downstream of the thin front layer, so that  $c_1$ ,  $c_2$ , and  $c_3$  in Eq. (22) are determined from the downstream condition as  $c_1 = \widehat{\rho}_+ \widehat{v}_+$ ,  $c_2 = (\widehat{T}_+/\widehat{v}_+) + 2\widehat{v}_+$ , and  $c_3 = \widehat{v}_+^2 + [(5+\delta)/2]\widehat{T}_+$ . However, these downstream quantities are expressed in terms of the upstream quantities by Eq. (21). Therefore, we can express  $c_1$ ,  $c_2$ , and  $c_3$  using the upstream quantities as

$$c_1 = \widehat{v}_-, \quad c_2 = \frac{1}{\widehat{v}_-} + 2\widehat{v}_-, \quad c_3 = \widehat{v}_-^2 + \frac{5+\delta}{2}. \quad (25)$$

Using these relations and the ratio of specific heats  $\gamma = (5+\delta)/(3+\delta)$ , we can transform Eq. (24) as follows:

$$\widehat{v}_1^2 (\widehat{v}_* - \widehat{v}_1) \frac{d\widehat{v}_1}{dy_1} = -\frac{3(\gamma+1)}{16} \widehat{v}_- \widehat{A}_c(\widehat{T}) (\widehat{v}_- - \widehat{v}_1) (\widehat{v}_1 - \widehat{v}_+), \quad (26a)$$

$$\widehat{T}(\widehat{v}_1) = 1 + (\gamma-1) (\widehat{v}_1 - \widehat{v}_-) \left( \widehat{v}_1 - \frac{1+\widehat{v}_-^2}{\widehat{v}_-} \right), \quad (26b)$$

where  $\widehat{v}_*$  and  $\widehat{v}_+$  (downstream velocity) are expressed in terms of  $\widehat{v}_-$  as

$$\widehat{v}_* = \frac{5}{16} \frac{1+2\widehat{v}_-^2}{\widehat{v}_-}, \quad \widehat{v}_+ = \frac{(\gamma-1)\widehat{v}_-^2 + \gamma}{(\gamma+1)\widehat{v}_-}. \quad (27)$$

Let us consider the integration of Eq. (26), with an initial condition  $\widehat{v}_1 = \widehat{v}_0$  at  $y_1 = y_0$ , from  $y_1 = y_0$  to  $\infty$ . When  $\widehat{v}_1 < \widehat{v}_*$  and  $\widehat{v}_1 \in (\widehat{v}_+, \widehat{v}_-)$  (note that  $\widehat{v}_+ < \widehat{v}_-$ ),  $d\widehat{v}_1/dy_1$  is negative from Eq. (26). This range of  $\widehat{v}_1$  is not empty because  $\widehat{v}_+ < \widehat{v}_*$  for  $\gamma < 5/3$  and  $M_- > 1$ ; this can be seen readily from the relation

$$\frac{\widehat{v}_*}{\widehat{v}_+} = \frac{5}{16} (\gamma+1) \frac{2\widehat{v}_-^2 + 1}{(\gamma-1)\widehat{v}_-^2 + \gamma} = \frac{5}{8} \frac{\gamma+1}{\gamma} \frac{\gamma M_-^2 + 1}{(\gamma-1)M_-^2 + 2}. \quad (28)$$

Therefore, if the initial value  $\widehat{v}_0$  satisfies  $\widehat{v}_0 < \widehat{v}_*$  and  $\widehat{v}_0 \in (\widehat{v}_+, \widehat{v}_-)$ , the solution  $\widehat{v}_1$  monotonically decreases as  $y_1$  increases and approaches  $\widehat{v}_+$ , which is an equilibrium point of  $\widehat{v}_1$  where  $d\widehat{v}_1/dy_1$  vanishes. This means that, with an appropriate choice of the initial value  $\widehat{v}_0$ , the solution of Eq. (26) is expected to describe the velocity profile in the downstream range  $y_1 \in [y_0, \infty)$  of a shock wave. Once the solution  $\widehat{v}_1$

is obtained from Eq. (26), other quantities are obtained from Eq. (23). That is,

$$\widehat{\rho}(\widehat{v}_1) = \frac{\widehat{v}_-}{\widehat{v}_1}, \quad \widehat{T}_{\text{tr}}(\widehat{v}_1) = 1 + 2(\widehat{v}_- - \widehat{v}_1) \left( \widehat{v}_1 - \frac{1}{2\widehat{v}_-} \right), \quad (29a)$$

$$\widehat{T}_{\text{int}}(\widehat{v}_1) = 1 + \frac{8}{\delta} (\widehat{v}_1 - \widehat{v}_-) (\widehat{v}_1 - \widehat{v}_{**}), \quad (29b)$$

where  $\widehat{v}_{**}$  is the dimensionless downstream velocity of the shock wave when  $\theta = 0$ , which is defined as  $\widehat{v}_{**} = \widetilde{v}_+ / (2RT_-)^{1/2}$  with  $\widetilde{v}_+$  given by Eq. (12a) and thus is written in terms of  $\widehat{v}_-$  as  $\widehat{v}_{**} = (2\widehat{v}_-^2 + 5) / 8\widehat{v}_-$ . Equation (26) with the initial condition  $\widehat{v}_1(y_0) = \widehat{v}_0$  can be solved analytically. More specifically,  $\widehat{v}_1$  is obtained as the inverse function of the following function  $y_1(\widehat{v}_1)$ :

$$y_1(\widehat{v}_1) - y_0 = \frac{16}{3(\gamma + 1)\widehat{v}_-} \int_{\widehat{v}_1}^{\widehat{v}_0} \frac{u^2 (\widehat{v}_* - u)}{\widehat{A}_c(\widehat{T}(u)) (\widehat{v}_- - u) (u - \widehat{v}_+)} du. \quad (30)$$

Moreover, the integration can be carried out explicitly for special forms of  $\widehat{A}_c(\widehat{T})$ , such as  $\widehat{A}_c(\widehat{T}) = 1$ ,  $\sqrt{\widehat{T}}$ , and  $\widehat{T}$  (see Appendix D in [10]).

Let us now discuss the possible choices of the initial value  $\widehat{v}_0$  and the relation between the resulting solution  $\widehat{v}_1$  [and Eq. (29)] and the profiles of Type A, Type B, and Type C. Here, we note that  $\widetilde{M}_- < M_-$  holds because  $\widetilde{M}_- / M_- = \sqrt{3\gamma/5}$  and  $\gamma < 5/3$ .

- Case of  $\widetilde{M}_- < 1 < M_-$

Since  $\widetilde{M}_- = \sqrt{6/5}\widehat{v}_-$ , it follows from Eq. (27) that  $\widehat{v}_- < \widehat{v}_*$ . Therefore, the admissible range of the initial value  $\widehat{v}_0$ , i.e.,  $\widehat{v}_0 < \widehat{v}_*$  and  $\widehat{v}_0 \in (\widehat{v}_+, \widehat{v}_-)$ , reduces to just  $\widehat{v}_0 \in (\widehat{v}_+, \widehat{v}_-)$ . That is, we can take  $\widehat{v}_0$  as *almost*  $\widehat{v}_-$ , i.e.,  $\widehat{v}_0 = \widehat{v}_- - 0$ . Therefore, the solution  $\widehat{v}_1$  is expected to describe the whole profile of the velocity. Let us consider this point in more detail. We consider Eq. (30) for a fixed value of  $\widehat{v}_1$  in the middle of the profile,  $\widehat{v}_+ < \widehat{v}_1 < \widehat{v}_-$ . Then, we have the following estimate:

$$y_1(\widehat{v}_1) - y_0 > C_y(\widehat{v}_1) \int_{\widehat{v}_1}^{\widehat{v}_0} \frac{1}{\widehat{v}_- - u} du = C_y(\widehat{v}_1) [-\ln(\widehat{v}_- - \widehat{v}_0) + \ln(\widehat{v}_- - \widehat{v}_1)], \quad (31)$$

where

$$C_y(\widehat{v}_1) = \frac{16}{3(\gamma + 1)\widehat{v}_-} \frac{\widehat{v}_1^2 (\widehat{v}_* - \widehat{v}_0)}{\max_{\widehat{v}_1 \leq u \leq \widehat{v}_0} [\widehat{A}_c(\widehat{T}(u))] (\widehat{v}_0 - \widehat{v}_+)} > 0. \quad (32)$$

As the initial value  $\widehat{v}_0$  approaches the upstream velocity  $\widehat{v}_-$ , the coordinate  $y_1(\widehat{v}_1)$ , which expresses the coordinate  $y_1$  inside the shock profile, diverges to  $+\infty$ . To locate the shock profile in a more comfortable range with finite  $y_1$ , we need to shift the coordinate, or take the initial position  $y_0$  as  $-\infty$ . Theoretically, if we assume that  $\widehat{v}_0 \rightarrow \widehat{v}_-$  at  $y_1 \rightarrow -\infty$ , we obtain the whole profile of  $\widehat{v}_1$ , changing from  $\widehat{v}_-$  to  $\widehat{v}_+$ ,

in a range of finite  $y_1$ . Correspondingly,  $\hat{\rho}$  changes from  $\hat{\rho}(\hat{v}_-) = 1$  to  $\hat{\rho}(\hat{v}_+) = \hat{\rho}_+$ ,  $\hat{T}_{\text{tr}}$  changes from  $\hat{T}_{\text{tr}}(\hat{v}_-) = 1$  to  $\hat{T}_{\text{tr}}(\hat{v}_+) = \hat{T}_+$ , and  $\hat{T}_{\text{int}}$  changes from  $\hat{T}_{\text{int}}(\hat{v}_-) = 1$  to  $\hat{T}_{\text{int}}(\hat{v}_+) = \hat{T}_+$ . This solution corresponds to the whole profile of Type A.

- Case of  $\widetilde{M}_- = 1$

In this case, it follows from Eq. (27) that  $\hat{v}_* = \hat{v}_- = \sqrt{5/6}$ . Therefore, the admissible range of the initial value  $\hat{v}_0$  is still  $\hat{v}_0 \in (\hat{v}_+, \hat{v}_-)$ . However, Eq. (30) reduces to

$$y_1(\hat{v}_1) - y_0 = \frac{16}{3(\gamma + 1)\hat{v}_-} \int_{\hat{v}_1}^{\hat{v}_0} \frac{u^2}{\widehat{A}_c(\widehat{T}(u))(u - \hat{v}_+)} du. \quad (33)$$

Since the integrand does not have a singularity at  $u = \hat{v}_-$ , the integral takes a finite value at  $\hat{v}_0 = \hat{v}_-$  for a fixed value of  $\hat{v}_1$  in the middle of the profile,  $\hat{v}_+ < \hat{v}_1 < \hat{v}_-$ . This means that  $y_0$  can be a finite value, say  $y_0 = 0$ , and the velocity profile locates in a range with finite  $y_1$ . Therefore, the solution  $\hat{v}_1$  can describe the whole velocity profile  $\hat{v}_- \rightarrow \hat{v}_+$  in the range  $y_1 \in [y_0, \infty)$ . From Eq. (26), we observe that

$$\left. \frac{d\hat{v}_1}{dy_1} \right|_{y_1=y_0} = -\frac{3(\gamma + 1)}{16} \widehat{A}_c(1) \frac{\hat{v}_- - \hat{v}_+}{\hat{v}_-} < 0. \quad (34)$$

This means that the profile of the velocity suddenly start at  $y_1 = y_0$  with a finite gradient and approaches  $\hat{v}_+$  as  $y_1 \rightarrow \infty$ . In other words, the velocity profile exhibits a corner at  $y_1 = y_0$ . One can also show from Eq. (29) that  $d\hat{\rho}/dy_1 > 0$  and  $d\widehat{T}/dy_1 > 0$  at  $y_1 = y_0$ . Therefore, the profiles of  $\hat{\rho}$  and  $\widehat{T}$  also exhibit a corner. These observations are consistent with the numerical result shown in Fig. 3. This solution corresponds to the Type-B profile.

- Case of  $\widetilde{M}_- > 1$

Because  $\hat{v}_* < \hat{v}_-$  in this case, the admissible  $\hat{v}$  range for the initial value reduces to  $\hat{v}_0 \in (\hat{v}_+, \hat{v}_*)$ . Here, we should note that  $\hat{v}_+ < \hat{v}_{**} < \hat{v}_*$  holds. Therefore, we can take  $\hat{v}_{**}$ , which is the dimensionless downstream velocity of the shock wave when  $\theta = 0$ , as the initial value  $\hat{v}_0$ . Then, the solution  $\hat{v}_1$  describes the monotonic decrease from  $\hat{v}_{**}$  to  $\hat{v}_+$  as  $y_1$  varies from  $y_0$  to  $\infty$ . Correspondingly,  $\hat{\rho}$  changes from  $\hat{\rho}(\hat{v}_{**}) = \hat{\rho}_{**}$  to  $\hat{\rho}(\hat{v}_+) = \hat{\rho}_+$ ,  $\hat{T}_{\text{tr}}$  changes from  $\hat{T}_{\text{tr}}(\hat{v}_{**}) = \hat{T}_{**}$  to  $\hat{T}_{\text{tr}}(\hat{v}_+) = \hat{T}_+$ , and  $\hat{T}_{\text{int}}$  changes from  $\hat{T}_{\text{int}}(\hat{v}_{**}) = 1$  to  $\hat{T}_{\text{int}}(\hat{v}_+) = \hat{T}_+$ , where  $\hat{\rho}_{**} = \tilde{\rho}_+/\rho_-$  and  $\hat{T}_{**} = \tilde{T}_{\text{tr}+}/T_-$  are, respectively, the values of  $\hat{\rho}$  and  $\hat{T}_{\text{tr}}$  downstream of the shock wave with  $\theta = 0$  [cf. Eq. (12)]. This corresponds to the thick rear layer of the Type-C profile. To be more specific, we replace the thin front layer with a jump satisfying the Rankine–Hugoniot relations for  $\theta = 0$  and the thick layer with the solution corresponding to  $\hat{v}_1$  obtained here. In this way, we can describe the Type-C profile by the slowly-varying solution.

In summary, the slowly-varying solution, i.e.,  $\hat{v}_1$  obtained from Eq. (30) and

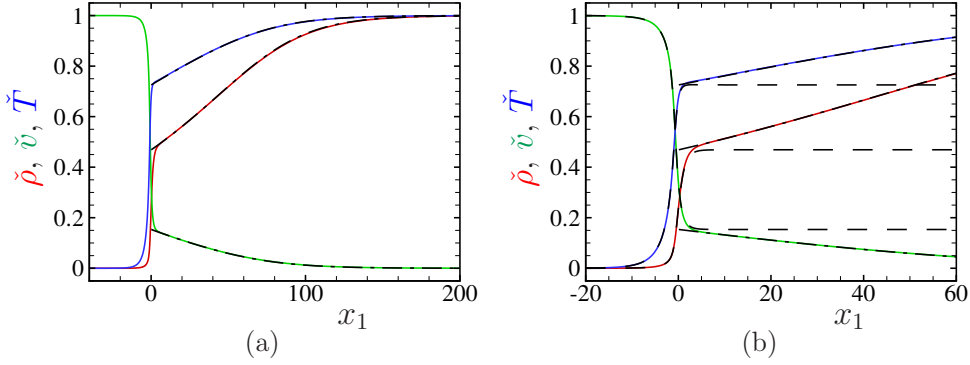


Fig. 5: Comparison between the profiles based on the slowly-varying solution and those of numerical solution. Profiles of  $\check{\rho}$ ,  $\check{v}$ , and  $\check{T}$  at  $M_- = 5$  for  $\delta = 4$ ,  $\text{Pr} = 0.761$ ,  $A_c = \text{const}$ , and  $\mu_b/\mu = 100$  are shown in the figure. (a) Profiles for  $-40 \leq x_1 \leq 200$ , (b) profiles for  $-20 \leq x_1 \leq 60$ . The red line indicates  $\check{\rho}$ , the green line  $\check{v}$ , and the blue line  $\check{T}$  of the numerical solution. The black dot-dashed line indicates the corresponding profiles obtained on the basis of the slowly-varying solution. In panel (b), the numerical solution of the ES model for  $\mu_b/\mu = \infty$  is also shown by the black dashed line.

the corresponding  $\hat{\rho}$ ,  $\hat{T}_{\text{tr}}$ , and  $\hat{T}_{\text{int}}$  in Eq. (29), can successfully describe the Type-A profile when  $\tilde{M}_- < 1 < M_-$ , the Type-B profile when  $\tilde{M}_- = 1$ , and the Type-C profile, with the help of the Rankine–Hugoniot relations for  $\theta = 0$  when  $\tilde{M}_- > 1$ .

In [13], the shock-wave structure of a polyatomic gas is investigated by a set of macroscopic equations that is derived by the extended thermodynamics [14] or from the Boltzmann equation by an appropriate moment closure [14, 15] (see also [13]). The macroscopic equations expressed in terms of the slowly-varying variable  $y_1$  in Eq. (13) are essentially the same as our equations (18).

## 6.2 Comparison with numerical results

Let us compare the slowly-varying solution with the numerical solutions. For our  $\text{CO}_2$  gas with varying  $\mu_b/\mu$ , the values  $\mu_b/\mu = 100$  and  $1000$  gives  $\theta = 5.00\dots \times 10^{-3}$  and  $5.00\dots \times 10^{-4}$ , respectively, which are quite small. Therefore, we can expect that the leading-order slowly-varying solution obtained in Sec. 6.1 describes the shock profile accurately. To confirm this statement, we consider the case of  $\mu_b/\mu = 100$ , for which the leading-order solution should be less accurate than the case of  $\mu_b/\mu = 1000$ , and make some comparisons. In Figs. 5–7 below,  $x_1 = 0$  is set in the same way as in Figs. 1, 3, and 4, respectively, for the numerical solution. Then, the profiles obtained by the slowly-varying solution is shifted in such a way that the point at which  $\check{\rho} = 0.5$  coincides with that of the numerical solution.

Figure 5 shows the profiles of  $\check{\rho}$ ,  $\check{v}$ , and  $\check{T}$  at  $M_- = 5$  and for  $\mu_b/\mu = 100$ . Figure 5(b) is a magnified figure of Fig. 5(a). The colored lines show the numerical solution

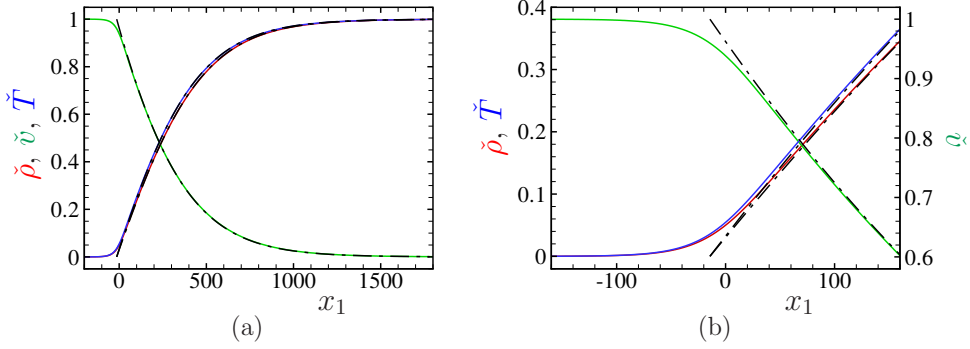


Fig. 6: Comparison between the profiles based on the slowly-varying solution and those of numerical solution. Profiles of  $\check{\rho}$ ,  $\check{v}$ , and  $\check{T}$  at  $M_- = 1.138\dots$  ( $\widetilde{M}_- = 1$ ) for  $\delta = 4$ ,  $\text{Pr} = 0.761$ ,  $A_c = \text{const}$ , and  $\mu_b/\mu = 100$  are shown in the figure. (a) Profiles for  $-200 \leq x_1 \leq 1800$ , (b) profiles for  $-160 \leq x_1 \leq 160$ . The red line indicates  $\check{\rho}$ , the green line  $\check{v}$ , and the blue line  $\check{T}$  of the numerical solution. The black dot-dashed line indicates the corresponding profiles obtained on the basis of the slowly-varying solution.

obtained in Sec. 5: the red line indicates  $\check{\rho}$ , the green line  $\check{v}$ , and the blue line  $\check{T}$ . The black dot-dashed line indicates the profile of the thick rear layer obtained on the basis of the Rankine–Hugoniot relations for  $\mu_b/\mu = \infty$  [cf. Eq. (12)] and the slowly-varying solution corresponding to Eq. (30) in the case of  $\widetilde{M}_- > 1$  (see Sec. 6.1). In Fig. 5(b), the numerical result for  $\mu_b/\mu = \infty$  is also shown by the black dashed line. As one can see, the slowly-varying solution describes perfectly the profiles in the thick rear layer. Needless to say, Fig. 5 corresponds to Type-C profile.

The comparison of the profiles at  $M_- = 1.138\dots$  ( $\widetilde{M}_- = 1$ ) and for  $\mu_b/\mu = 100$  is made in Fig. 6. Figure 6(b) is a magnified figure of Fig. 6(a). Note that the scale of  $\check{v}$  is shown on the right side in Fig. 6(b). In this case, the slowly-varying solution based on Eq. (30) gives a profile that starts suddenly with a corner, as shown by the dot-dashed lines in Fig. 6(b). It agrees with the numerical solution on the whole though there is a visible difference in the magnified figure, Fig. 6(b). The numerical solution gives profiles that start smoothly without a corner. However, as  $\mu_b/\mu$  becomes large, say 1000, the start of the profiles becomes sharper, and the difference between the numerical and slowly-varying solutions becomes invisible. This corresponds to Type-B profile.

Figure 7 shows the comparison of the profiles at  $M_- = 1.05$  and for  $\mu_b/\mu = 100$ . In this case, the agreement between the numerical and slowly-varying solutions is good even in the magnified Fig. 7(b). This corresponds to Type-A profile.

In this subsection, we compared the numerical and slowly-varying solutions for our  $\text{CO}_2$  gas with varying  $\mu_b/\mu$  when it is smaller than the real value, i.e.,  $\mu_b/\mu = 100$ , and confirmed the agreement. It should be emphasized that we have much better agreement for the real  $\text{CO}_2$  gas with  $\mu_b/\mu$  of the order of 1000.



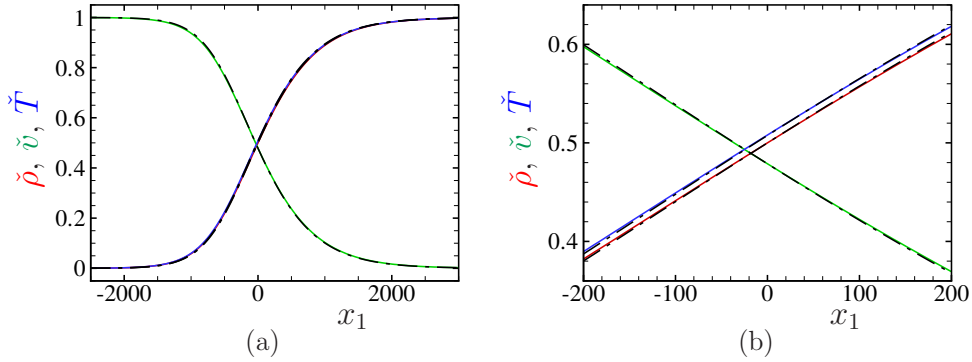


Fig. 7: Comparison between the profiles based on the slowly-varying solution and those of numerical solution. Profiles of  $\check{\rho}$ ,  $\check{v}$ , and  $\check{T}$  at  $M_- = 1.05$  for  $\delta = 4$ ,  $\text{Pr} = 0.761$ ,  $A_c = \text{const}$ , and  $\mu_b/\mu = 100$  are shown in the figure. (a) Profiles for  $-2500 \leq x_1 \leq 3000$ , (b) profiles for  $-200 \leq x_1 \leq 200$ . See the caption of Fig. 6.

## 7 Concluding remarks

In the present study, we investigated the structure of a standing shock wave in a polyatomic gas with a large bulk viscosity on the basis of the polyatomic version of the ES model for the Boltzmann equation. It is known that  $\text{CO}_2$  gas has a large value of the ratio of the bulk viscosity to the viscosity ( $\mu_b/\mu$ ), which is of the order of 1000. Therefore, we considered an artificial  $\text{CO}_2$  gas with the same properties as  $\text{CO}_2$  gas except that  $\mu_b/\mu$  takes arbitrary values and investigated its behavior as  $\mu_b/\mu$  increases up to 2000 to understand the properties of the shock profiles when  $\mu_b/\mu$  is large. The study was motivated by the recent results based on the extended thermodynamics [6, 7].

We first carried out direct numerical computations of the ES model and obtained the profiles of the macroscopic quantities inside the shock wave accurately. In this step, we were able to reproduce the Type-A, Type-B, and Type-C profiles defined in [6], that is, Type-A profile is a profile almost symmetric with respect to the center for each macroscopic quantity, Type-B profile is the profile that is nonsymmetric and has a corner upstream, and Type-C profile is the profile consisting of a thin upstream layer with a sharp change and a thick downstream layer with a slow change. We observed that as the ratio  $\mu_b/\mu$  increases, the thin front layer in Type-C profile does not change, whereas the thickness of the thick rear layer increases indefinitely. In the limit when  $\mu_b/\mu \rightarrow \infty$ , the shock wave reduces to the thin upstream layer only and its downstream state approaches a uniform equilibrium state satisfying the different Rankine–Hugoniot relations [Eq. (12)] that hold when  $\mu_b/\mu = \infty$ .

Then, motivated by the numerical results, we tried to describe the behavior of the thick rear layer of Type-C profile by a slowly-varying solution of the ES model, the length scale of which is of the order of  $\mu_b/\mu$  (or the inverse of the parameter  $\theta$  appearing in the ES model). Carrying out an asymptotic analysis for small  $\theta$  (or

large  $\mu_b/\mu$ ) using a Hilbert-type expansion, we derived a simple set of ordinary differential equations for the macroscopic quantities, which can be solved analytically. We showed that Type-C profile can be described by this slowly-varying solution correctly if its upstream condition is set to be the downstream condition of the Rankine–Hugoniot relations for  $\mu_b/\mu = \infty$ . In addition, we showed that the slowly-varying solution can also describe the entire Type-A and Type-B profiles correctly.

## References

- [1] M. N. Kogan, *Rarefied Gas Dynamics*, Plenum, New York, 1969.
- [2] J. H. Ferziger and H. G. Kaper, *Mathematical Theory of Transport Processes in Gases*, North Holland, Amsterdam, 1972.
- [3] C. Cercignani, *The Boltzmann Equation and Its Applications*, Springer, Berlin, 1988.
- [4] G. A. Bird, *Molecular Gas Dynamics and the Direct Simulation of Gas Flows*, Oxford University Press, Oxford, 1994.
- [5] Y. Sone, *Molecular Gas Dynamics: Theory, Techniques, and Applications*, Birkhäuser, Boston, 2007.
- [6] S. Taniguchi, T. Arima, T. Ruggeri, and M. Sugiyama, Thermodynamic theory of the shock wave structure in a rarefied polyatomic gas: Beyond the Bethe–Teller theory, *Phys. Rev. E*, **89**, 013025 (2014).
- [7] S. Taniguchi, T. Arima, T. Ruggeri, and M. Sugiyama, Overshoot of the non-equilibrium temperature in the shock wave structure of a rarefied polyatomic gas subject to the dynamic pressure, *Int. J. Non-Linear Mech.*, **79**, 66–75 (2016).
- [8] P. Andries, P. Le Tallec, J.-P. Perlat, and B. Perthame, The Gaussian-BGK model of Boltzmann equation with small Prandtl number, *Eur. J. Mech. B/Fluids*, **19**, 813–830 (2000).
- [9] S. Brull and J. Schneider, On the ellipsoidal statistical model for polyatomic gases, *Continuum Mech. Thermodyn.*, **20**, 489–508 (2009).
- [10] S. Kosuge and K. Aoki, Shock-wave structure for a polyatomic gas with large bulk viscosity, *Phys. Rev. Fluids*, **3**, 023401 (2018).
- [11] F. J. Uribe, E. A. Mason, and J. Kestin, Thermal conductivity of nine polyatomic gases at low density, *J. Phys. Chem. Ref. Data*, **19**, 1123–1136 (1990).
- [12] G. Emanuel, Bulk viscosity of a dilute polyatomic gas, *Phys. Fluids A*, **2**, 2252–2254 (1990).

- [13] M. Pavić-Čolić, D. Madjarević, and S. Simić, Polyatomic gases with dynamic pressure: Kinetic non-linear closure and the shock structure, *Int. J. Non-Linear Mech.* **92**, 160–175 (2017).
- [14] T. Arima, S. Taniguchi, T. Ruggeri, and M. Sugiyama, Extended thermodynamics of real gases with dynamic pressure: an extension of Meixner’s theory, *Phys. Lett. A* **376**, 2799–2803 (2012).
- [15] T. Ruggeri, Non-linear maximum entropy principle for a polyatomic gas subject to the dynamic pressure, *Bulletin of the Institute of Mathematics, Academia Sinica (New Series)*, **11**, 1–22 (2016).